A Workflow for Identifying Viable Crystal Structures with Partially Occupied Sites Applied to Solid Electrolyte: Cubic $Li_7La_3Zr_2O_{12}$

Julian Holland,[†,‡] Tom Demeyere,[†] Arihant Bhandari,[†,‡] Felix Hanke,[¶] Victor Milman,[¶] and Chris-Kriton Skylaris[*,†,‡]

†*School of Chemistry, University of Southampton, Southampton SO17 1BJ, UK*

‡*The Faraday Institution, Quad One, Becquerel Avenue, Harwell Campus, Didcot, OX11*

¶*BIOVIA, 22 Cambridge Science Park, Milton Road, Cambridge, Cambridgeshire, CB4 0FJ, UK*

E-mail: C.skylaris@soton.ac.uk

Abstract

Experimental and theoretical works have, to date, been unable to uncover the ground state configuration of prominent solid electrolyte candidate cubic $Li_7La_3Zr_2O_{12}$ (c-LLZO). Computational studies rely on an initial low-energy structure as a reference point. In this study, we present a methodology to identify energetically favourable configurations of c-LLZO, enabling the isolation of low-energy structures, for a crystallographically predicted structure. We begin by eliminating structures that involve overlapping Li atoms based on nearest neighbour counts. We further reduce the configuration space by eliminating symmetry images from all remaining structures. This is followed up with a machine learning-based energetic ordering of all remaining structures. By considering the geometrical constraints that emerge from this methodology we determine that a large portion of previously reported structures may not be feasible or stable. The method developed here could be extended to other ion conductors and partially occupied crystals. Furthermore, we provide all structures generated in a freely accessible database with the aim to improve accuracy and reproducibility in future c-LLZO research.

Main Text

Solid Electrolytes for Li-ion batteries promise higher energy density, improved safety, longer lifetimes,[1] and reduced production costs compared to the current generation of liquid electrolyte commercial cells.[2,3] Electrochemical and chemomechanical stability present a significant issue for a number of superionic solid state conductors;[4] Dendrite formation through the electrolyte causing the batteries to short-circuit has been reported even for the most stable solid electrolytes.[5–9] $Li_7La_3Zr_2O_{12}$ (LLZO) has the best interfacial stability of all popular fast ion conducting solid electrolytes against metallic Li.[10] LLZO has two primary polymorphs, the highly conducting disordered cubic LLZO (c-LLZO) and ordered tetragonal LLZO (t-LLZO) with a Li diffusivity over two orders of magnitude smaller than the cubic phase.[11,12]

c-LLZO has a Hermann-Maguin space group of $Ia\bar{3}d$ with Li atoms partially occupying the $24d$ and $96h$ sites (c.f. Figure 1b). c-LLZO is not stable at room temperature but has been stabilised with a number of substitutional dopants on $24d$ sites[13–16] The $24d$ site is tetrahedral and the $96h$ site occurs at a tetrahedral/octahedral interface.

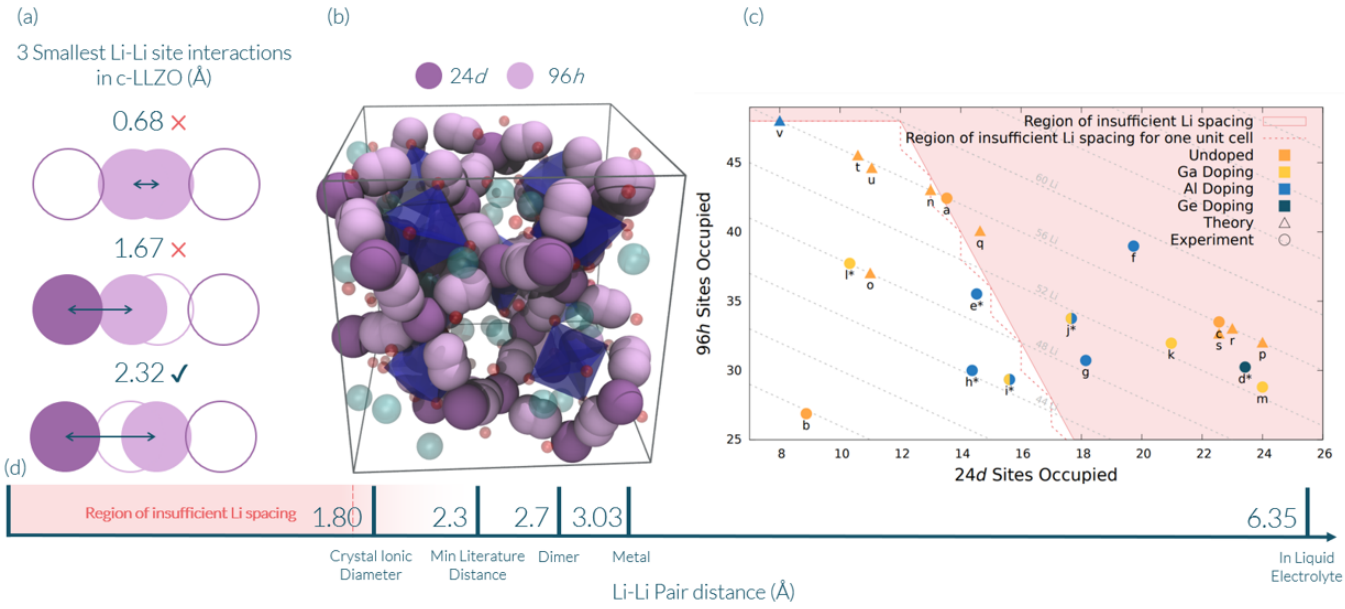

Figure 1: (a) examples of the 3 smallest site interactions from the centre of each atom. First and second neighbour Li sites are too close and cannot simultaneously contain a Li atom. (b) a unit cell of c-LLZO with all $24d$ (dark purple) and $96h$ (light purple) sites highlighted. O and La are represented by red and green spheres respectively, the Zr atoms are represented by the blue polyhedra. (c) shows experimental and theoretical site assigments and/or starting structures in the literature: a,[17] b,[13] c,[12] d,[18] e,[19] f,[20] g,[21] h,[22] i,[22] j,[22] k,[23] l,[24] m,[21] n,[7–9,25–29] o,[30] p,[31] q,[32] r,[33] s,[34] t,[34] u.[35] * indicates that experimental assignments used neutron diffraction, no * means the experimental assignments used x-ray diffraction. The region in red indicates the $24d$:$96h$ ratios that cannot exist without a Li-Li interaction below the crystal ionic diameter. The data for this image is provided in the supporting information (Tables S1 and S2). (d) a scale showing the important Li-Li interactions distances recorded in the literature: Crystal Ionic Diameter,[36] Min Literature Distance,[37] Metal,[38] Dimer (in a vacuum) (c.f. figure S4), In Liquid Electrolyte (average Li-Li distance)[39] as well as our chosen cutoff point at 1.7 Å (red dashed line).

Despite the material's technological relevance and intensive study[35,40–44] there is no consensus of c-LLZO's Li occupancy (c.f. Figure 1c). Here, we present a combinatorial study to find and rank all possible Li site occupancies. Previous computational studies often use

one of the experimental values in Figure 1 as a starting point to obtain an idealised unit cell using a variety of methods (c.f. Table S2). The range of predicted structures in the literature indicates some disagreement about the ground state. Without knowing if the structures used are close to the ground state, more complicated thermodynamic and observable, properties calculated from these structures may not be well described.

To find the most stable structures we intend to produce all possible structures of a c-LLZO unit cell and order them energetically to ascertain the presence of a significant energy difference in choice of structure. We also hope to elicit whether some of the structural properties, such as the $24d$:$96h$ ratio, are indicative of a structure's energy. We neglect to include the $48g$ site that occurs between the $96h$ sites as it is not reported in most refinements we find (c.f. Table S1 for references). The structures produced in this work are be published alongside our results (c.f. Supporting Information (SI) section) in the hope that we can provide further clarity and improve reproducibility in this field of research.

The number of ways to populate 120 sites with 56 Li is $\binom{120}{56} \approx 7.4 \times 10^{34}$, rendering a brute-force combinatorial method unviable. To reduce this configuration space, we begin by eliminating all overlapping Li atoms (c.f. Figure 1a)[45] by imposing a minimal Li-Li distance. Here, we use 1.7 Å (c.f. SI section) which is less than 2 times the ionic radius of a Li atom and smaller than the minimum distance in t-LLZO (2.56 Å),[46] and significantly less than Li-Li distances in metallic Li. In practice, any minimal distance between 1.67 Å and 2.3 Å would be suitable for a numerical implementation.

This constraint on allowed Li-Li distances immediately limits the physically possible $24d$:$96h$ ratios. To describe the possible structures available under this simple geometric constraint, we outline the two major consequences this limit imposes.

1. A maximum of 48 out of $96h$ sites can be occupied at anyone time: each $96h$ site exists as a pair within 0.68 Å of each other, at most one site can contain a Li atom.

2. Each of the $24d$ occupation eliminates 4 out of $96h$ sites as they are within 1.67 Å of this site.

We can use this information to narrow the range of Li site occupations

$$y_{96h\ \text{Occupancy}} \leq \frac{N_{96h\ \text{sites}}}{2}, \tag{1}$$

$$y_{96h\ \text{Occupancy}} \leq N_{96h\ \text{sites}} - 4x_{24d\ \text{Occupancy}}, \tag{2}$$

where $N_{96h\ \text{sites}}$ is the number of total $96h$ sites, $y_{96h\ \text{Occupancy}}$ is the number of $96h$ sites occupied, and $x_{24d\ \text{Occupancy}}$ is the number of $24d$ sites occupied. The area described in Eqs. 1 and 2, the unshaded area in Figure 1c, is the region with sufficient Li spacing at a given Li concentration. The full region is shown in figure S1. Outside of this area the structures, by necessity, will have a Li-Li interaction smaller than what we would expect to find in reality. For the stoichiometrically predicted case (56 Li atoms per unit cell), we observe that $8 \leq x_{24d\ \text{Occupancy}} \leq 13.\dot{3}$. This means the only stoichiometric $24d$:$96h$ ratios possible, for a single unit cell, are 8:48, 9:47, 10:46, 11:45, 12:44, and 13:43. This is how we refer to specific ratios throughout the rest of this communication.

Figure 1c shows a significant number of studies report structures that imply overlapping Li atoms with Li-Li distances smaller than 1.7 Å. For example, a structure with a $24d$:$96h$ ratio of 17:39 has a population of 17 $24d$ sites necessitating that 68 (4×17) out of the 96 h sites will fall within 1.7 Å of an occupied $24d$ site. Trying to distribute 39 Li atoms amongst the remaining 28 ($96 - 68$) sufficiently spaced $96h$ sites is impossible so 11 of these Li atoms will occupy sites within 1.7 Å of another Li atom.

Having established the possible $24d$:$96h$ ratios, we can generate all allowed structures. We initially generate all possible $24d$ permutations for a given $24d$ occupancy, eliminating directly neighbouring $96h$ sites from consideration. We then populate the remaining $96h$ sites such that no two nearest neighbours are occupied simultaneously. The number of structures for each $24d$:$96h$ ratio, for one unit cell, are given in Table 1. We use the crystal structure sites reported by Buschmann et al.[19] as our framework to perform our generation in.

This method will generate all possible structures, approximately 2.3×10^8, including

symmetry-equivalent duplicates. To further reduce our large data set to unique conformations, we construct the upper triangular connectivity matrix of the Li sub-lattice for each structure. We define a connectivity matrix as the distances between each Li atom to every other Li atom. The matrix is then flattened and sorted to ensure uniformity in all matrices. This preprocessing of our structures decreases the memory required to store our structures compared to the full atomic structure of the crystal. A direct comparison of all structures to check symmetry would be computationally costly. We use local sensitive hashing (LSH) [47] to perform fast approximate similarity searches with further lower memory requirements than the unhashed data. The use of LSH optimises the pairwise comparison from scaling at $\mathcal{O}(N^2)$ to $\mathcal{O}(N)$, where N is the number of structures. This symmetry comparison method is designed to work for large data sets of similar data, allowing us to perform symmetry checks on over 100 million structures in a reasonable time frame and attainable memory requirements, something that would be impractical to attempt with conventional methods. [48–50] The trade-off for increased speed and lower memory costs is the high specificity of the method. In practice, this method is limited to comparison of monoatomic sub-lattices with predefined positions.

We validated this method for both 13:43 and 12:44 ratios, see the supporting information for further discussion. Employing this technique we find that only approximately 1% of our structures are symmetrically unique, allowing a reduction by a further factor of approximately 100 (c.f. Table 1).

Table 1: The total number of c-LLZO structures for every possible $24d$:$96h$ ratio after limiting to the specific $24d$:$96h$ ratio(s) (c.f. SI section), mandating all Li-Li interactions must be greater 1.7 Å, and ensuring the structures generated are symmetry unique

$24d$:$96h$	Ratio Limited	>1.7 Å spacing	Symmetry unique
8:48	1.8×10^{25}	80,019,456	816,454
9:47	9.3×10^{23}	98,304,000	905,216
10:46	4.4×10^{22}	41,754,624	366,971
11:45	1.9×10^{21}	7,176,192	65,958
12:44	7.6×10^{19}	427,176	4,162
13:43	2.6×10^{18}	1,056	11
Total	1.9×10^{25}	227,682,504	2,158,772

Having reduced the configuration space to around 2×10^6 structures (c.f. Table 1) we can energetically order our structures. To achieve this in a reasonable time frame, we perform DFT calculations on small subsets of the total number of structures. The results are then used to fit a multiple linear regression (MLR) model. The DFT calculations were performed on 2 major subsets of structures. The first subset was the 200 energetically lowest structures according to the COMPASSIII forcefield,[51] (c.f. SI section). The second subset was a random selection of approximately 1000 structures across the entire configuration space to ensure good coverage. In total 1235 single point DFT calculations were performed.

All DFT calculations were performed with the ONETEP code, where the computational cost scales linearly with the number of atoms as opposed to cubic scaling in conventional DFT.[52,53] We use the PBE GGA exchange correlation functional[54] and a kinetic energy cutoff of 830 eV. Further details including all input files can be found in SI sections and .

We assume the base LaZrO structure remains relatively unchanged with each configuration and therefore the majority of all energetic changes are due to Li placement. Therefore, an expression of all types of Li interactions would be a sufficient descriptor for predicting the energies of c-LLZO structures. The DFT energies were paired with a numerical rep-

resentation of the structure and fit using a multiple linear regression model (MLR). The structures were represented by a frequency occurrence list of all possible Li-Li interactions. This representation is a reformulation of the connectivity matrix of the Li sub-lattice used for the symmetry reduction described above. The data were split into test and training sets with a 1:3 ratio.

We found through applying this model to our test set a correlation of 0.9996 (c.f. Figure 2a) with DFT energies with a mean average error of 0.0325 eV.

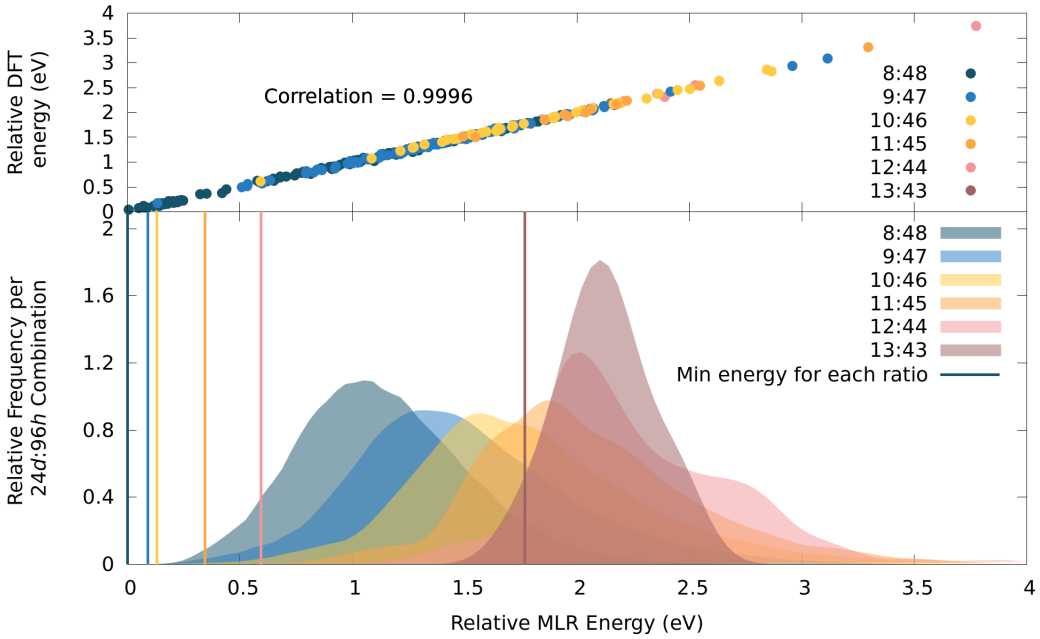

Figure 2: (above) the parity plot of the test set of ONETEP total energies compared to MLR predicted energies for each $24d$:$96h$ ratio. (below) The relative frequency of energy occurrences for each $24d$:$96h$ ratio.

All structures are found to occur within a range of 5.8 eV of our lowest energy structure. 19 out of the 20 lowest energy structures have a ratio of 8:48 (c.f. Figure 2b) with the 19^{th} lowest being 9:47. The average energy for all structures occurs at 1.47 eV higher than the ground state structures. The average energy for each ratio increases with increasing $24d$ occupancy, indicating an energetic preference to avoid $24d$ occupation where possible. There are four structures, all 8:48, within 0.026 eV (1 kT at 298 K) of the lowest energy structure we find (c.f. Figure 3). The four lowest energy have very similar atomic coordinates, all

have the same $24d$ configuration with only slight variations in the $96h$ configuration. We perform geometry optimisation calculations on the final four structures and find the energy gap between them narrows further.

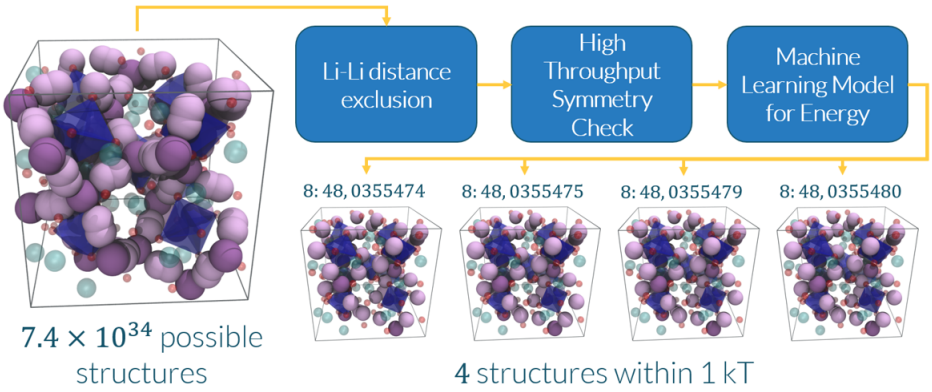

Figure 3: The workflow we employ to find our 4 final structures from given occupancies. Above each structure is its respective $24d$:$96h$ ratio and unique identity number in the c-LLZO database we have built (c.f. SI section)

We note that our energetic ordering procedure does not include entropic contributions and assumes a reasonable retention of ordering upon geometry relaxation, which are both approximations. We have tested the effect of geometry relaxation on a small dataset of 20 structures (c.f. SI section). A large-scale energy prediction of the geometry optimised structures falls outside the scope of this communication.

In summary, we have created a fast evaluation procedure to generate and energetically order all crytallographically predicted structures for crystals with partially occupied sites. We have used the basis of this procedure, disallowing structures with atoms too close to each other, to highlight that a large proportion of experimental and theoretical literature are predicting or working with structures that are not reflective of a real system (c.f. Figure 1). It is our hope that in providing all possible structures so we can bring further accuracy and reproducibiliy to future computational LLZO research.

Acknowledgements

We would like to thank Davide Sarpa, Jacek Dziedzic, Benedict Saunders, and Brad Ayers for proof reading, calculation assistance, and aesthetic choices. We also thank Dr. Johan Carlsson, Dr. Hamidreza Hajiyani, Elizabeth Ojogbede for providing expert advice and probing questions that resulted in a stronger piece of research. We thank Dr. Samantha Kanza for their assistance with data processing. We thank Dr. Mark Light for providing guidance with terminology. We are grateful to the UK Materials and Molecular Modelling Hub for computational resources, which is partially funded by EPSRC (EP/P020194/1 and EP/T022213/1). The authors acknowledge the use of the IRIDIS High Performance Computing Facility, and associated support services at the University of Southampton, in the completion of this work. This work used the ARCHER2 UK National Supercomputing Service (https://www.archer2.ac.uk). J. H. would like to thank BIOVIA for an EPSRC iCASE PhD funding. This work was supported by the Faraday Institution (grant number FIRG059).

Supplementary Material

Data

All structures, ONETEP input and output files, and codes used in this work can be accessed at

https://doi.org/10.5258/SOTON/D2704

Experimental Literature Summary Table

Table S1: All Experimental papers we could find that explicitly report the site occupancies of the 24*d* and 96*h* sites. The second column shows paper and the reported stoichiometry. The third column reports the method used with "X-ray" referring to some form of X-ray diffraction and "Neutron" referring to any presence of Neutron powder diffraction being present in the assignment. The remaining columns are taken directly from the respective papers and standardised to report the proportion of sites occupied out of total sites and the amount of atoms that would result in for a full cubic structure
*** Ga occupies some of the La 24*c* sites. We have also approximated the 12*a* and 12*b* sites to be the same as the 24*d* sites, as well as the two 48*e* Li sites to be 96*h* so we can compare with the other structures.**
† a significant portion of Li reported was unassigned

	Paper Assigned Stoichiometry	Method	Li 24*d* Fraction (Occupancy)	Dopant 24*d* Fraction (Occupancy)	Li 96*h* Fraction (Occupancy)	Total Assigned Sites Occupied
a	Xie et al.[17] $Li_7La_3Zr_2O_{12}$	X-ray	0.564 (13.53)	-	0.442 (42.43)	55.96
b	Geiger et al.[13] $Li_{4.47}La_3Zr_2O_{12}$	X-ray	0.37 (8.88)	-	0.28 (26.88)	35.76
c	Awaka et al.[12] $Li_7La_3Zr_2O_{12}$	X-ray	0.94 (22.56)	-	0.349 (33.504)	56.08
d	Brugge et al.[18] $Li_{6.6}Ge_{0.1}La_3Zr_2O_{12}$	Neutron	0.943 (22.64)	Ge 0.033 (0.8)	0.315 (30.24)	53.68
e	Buschmann et al.[19] $Li_{6.06}Al_{0.2}La_3Zr_2O_{12}$	Neutron	0.54 (12.96)	Al 0.0653 (1.44)	0.37 (35.52)	49.92
f	Hiebl et al.[20] $Li_7Al_{0.33}La_3Zr_2O_{12}$	X-ray	0.712 (17.08)	Al 0.11 (2.64)	0.406 (38.976)	58.696
g	Wagner et al.[21] $Li_{6.03}Al_{0.08}La_3Zr_2O_{12}$	X-ray	0.68 (16.32)	Al 0.076 (1.824)	0.32 (30.72)	48.864
h	Rettenwander et al.[22†] $Li_{5.5}Al_{0.19}La_3Zr_2O_{12}$	Neutron	0.54 (12.848)	Al 0.064 (1.528)	0.31 (30.0)	44.376
i	Rettenwander et al.[22†] $Li_{5.5}Al_{0.20}Ga_{0.05}La_3Zr_2O_{12}$	Neutron	0.57 (13.65)	Al 0.066 (1.584), Ga 0.016 (0.384)	0.31 (29.344)	44.96
j	Rettenwander et al.[22†] $Li_{6.3}Al_{0.12}Ga_{0.08}La_3Zr_2O_{12}$	Neutron	0.67 (16.08)	Al 0.039 (0.944), Ga 0.027 (0.64)	0.35 (33.752)	51.416
k	Robben et al.[23*] $Li_{6.25}Ga_{0.52}La_{2.67}Zr_2O_{12}$	X-ray	0.811 (19.464)	Ga 0.063 (1.512)	0.315 (31.68)	52.656
l	Howard et al.[24] $Li_{5.5}Ga_{0.5}La_3Zr_2O_{12}$	Neutron	0.263 (6.312)	Ga 0.167 (4.008)	0.393 (37.728)	48.048
m	Wagner et al.[21] $Li_{6.58}Ga_{0.016}La_3Zr_2O_{12}$	X-ray	0.984 (23.616)	Ga 0.016 (0.384)	0.30 (28.8)	52.8

Theoretical Literature Summary Table

Table S2: All theoretical studies we could find who explicitly report their 24*d*:96*h* ratio and a brief summary of how their structures were generated. If a dopant is present it is included in the total 24*d*:96*h* ratio. We should note that under the majority of these schemes the 24*d*:96*h* ratio is likely not maintained after a allowing their structure to relax or move but the final ratio is rarely reported.
† Methodology is discussed further in text

	Paper	Li 24*d*:96*h* Ratio	Method
n	Tian et al.[9]	13:43	Use experimentally defined ratio[17] and generate 10 random structures
n	Gao et al.[8]	13:43	Use experimentally defined ratio[17] and generate 10 random structures
n	Yu et al.[25]	13:43	Unpublished electrostatic minimisation method
n	Thompson et al.[26]	13:43	Unpublished electrostatic minimisation method
n	Sharafi et al.[27]	13:43	npublished electrostatic minimisation method
n	Sharafi et al.[55]	13:43	Unpublished electrostatic minimisation method
n	Yu and Siegel[28]	13:43	perform a quasi random distribution of Li while keeping the occupancy of sites set
n	Barai et al.[7]	13:43	quasi-random distribution
n	Rettenwander et al.[29]	13:43 (Al)	Highest symmetry possible (for computational costs)
o	Zhang et al.[40]	11:37	Use experimentally defined ratio[12]* and geometry relaxes structure. Explanation is not given as to why the total number of Li changes
p	Xu et al.[30]	24:32	Fill all 24*d* sites, randomly distribute the 96*h* then perform a geometry relaxation
q	Jalem et al.[31]	14.64:40.05	AIMD at 1800 K
r	Meier et al.[32]	23:33	120 randomly distributed structures with ratio given by experiment[12]
s	Santosh et al.[33]	22.56:32.64	Started with experimental results[12] and optimised
t	Verduzco et al.[34]	10.59:45.51	Average occupancies after 25 ps of AIMD at 1273 and 1773 K
u	Verduzco et al.[34]	11.05:44.60	Average occupancies after 25 ps of AIMD at 1273 and 1773 K
v	Haarmann et al.[35]	8:48 (Al)	Combinatorial Software + AIMD†

Haarmann et al.[35] perform the most rigorous exploration of c-LLZO we found. They use the generalised combinatorial structure generation software, Supercell,[56] to generate a number of possible structures. However, due to the large amount of structures in typical c-LLZO cell, let alone a 2x2x2 supercell with an Al present, they limited the configuration space by only placing 48 Li exclusively at $48g$ sites and relying ab-initio molecular dynamics (AIMD) and geometry relaxation to move the Li into the correct 96h site. They allow the remaining Al and Li atoms the freedom of the 24d sites and generate all combinations and selecting the supercell with the lowest coulombic energy to proceed with. There are 2 issues with this procedure. Firstly, the choice of initial structure was mostly for convenience of a smaller phase space and a low energy structures is not necessarily guarenteed even with AIMD. Secondly, as we show in our supporting information using, the coulombic forces alone is not sufficient to energetically order c-LLZO structures.

Full Region of sufficient Li spacing

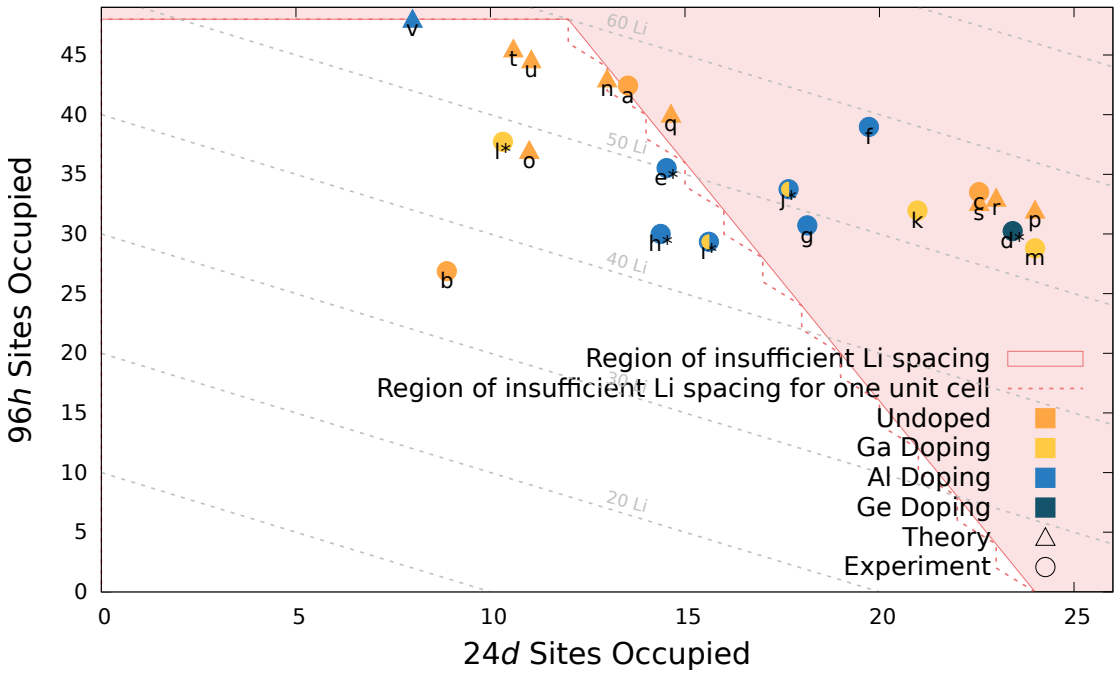

Figure S1: Zoomed out version of figure 1c showing the full area defined by equations 1 and 2.

Reduction of configuration space

The total number of structures (x) available for each $24d$:$96h$ ratio (i) for a single unit cell of a given Li occupancy (N), 56 for the stoichiometric case, can be calculated as

$$x_i = \binom{24}{i} + \binom{120 - 4i}{N - i} \tag{3}$$

For a stoichiometric unit cell we can calculate the total number of structures (x_{tot}) as

$$x_{\text{tot}} = \sum_{i=8}^{13} \binom{24}{i} + \binom{120 - 4i}{56 - i} \approx 1.93 \times 10^{25} \tag{4}$$

Alternative Energy Calculators

When attempting to energetically order all 2×10^6 structures we initially attempted to use already available methods such as force fields, which neglect explicitly modelling the electrons in favour of fitted potentials, or Density functional tight-binding (DFTB) which is based on a second-order expansion of the Kohn-Sham total energy functional.[57] These attempts were unsuccessful as they were unable to reproduce the energetic ordering produced by a sample DFT calculation batch. A comparison of the individual methods can be seen in figure S2.

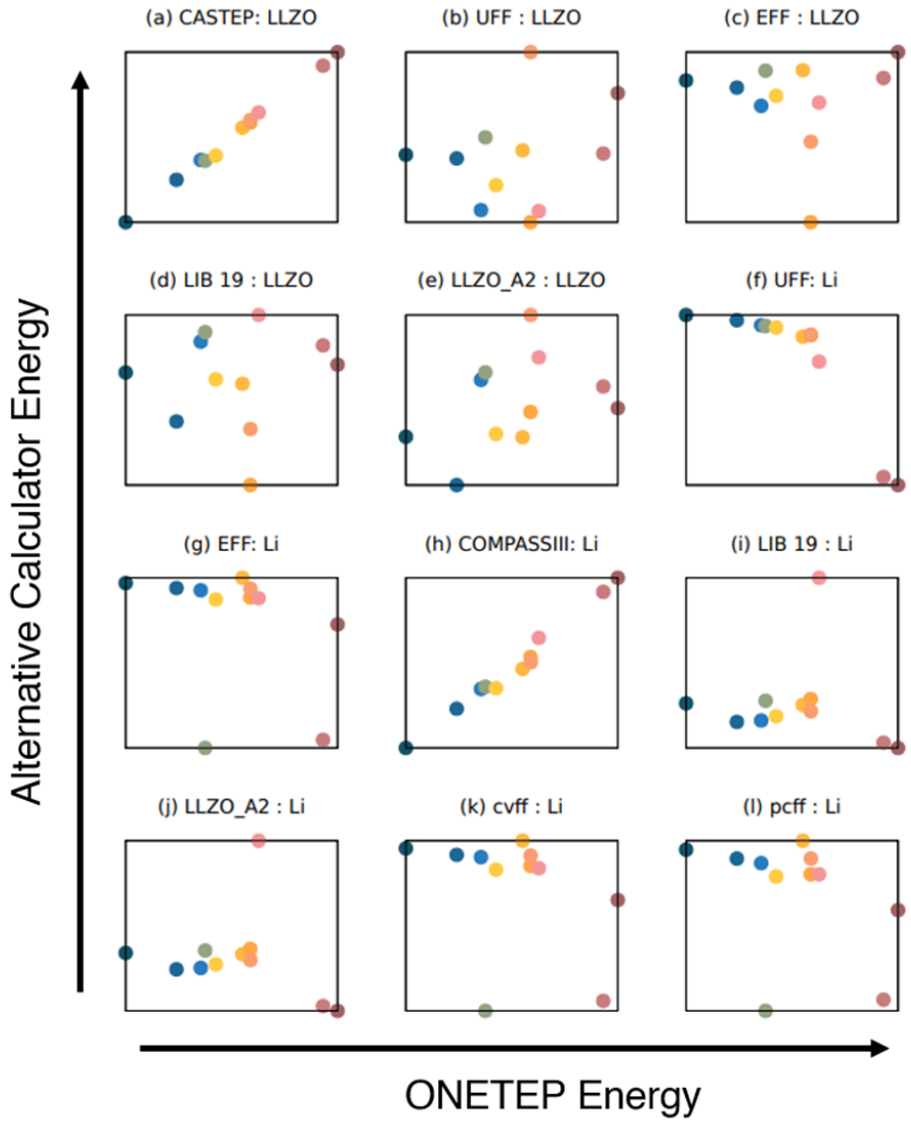

Figure S2: A comparison of the energetic ordering of all symmetry unique 13:43 structures for different energy calculators compared to our ONETEP calculations: (a) CASTEP:[58] DFT software used as our base line comparison, (b) and (f) FORCITE:[59] universal forcefield,[60] (c) and (g) FORCITE:[59] custom forcefield that exclusively considers the coulombic interaction of atoms, (d) and (i) DFTB+:[61] Slater-Koster library developed for Li ion batteries[59] and extended to include La and Zr interactions (if required) with data from the LLZO_A2 Slater-Koster library, (e) and (j) DFTB+:[61] unpublished custom parameterised Slater-Koster file specifically for LLZO, (h) FORCITE:[59] using the COMPASSIII forcefield,[62] (k) FORCITE:[59] using the cvff forcefield,[63] (l) FORCITE:[59] using the pcff forcefield[64]
Orderings with "Li" in the title indicate only the Li sublattice was used in the energy evaluation. "LLZO" indicates all atoms were used. Energy values are not included as they often (in the case of the Li only calculations) do not correspond to real systems. We are only interested in the ordering.

Due to the limited number of forcefields available with La and Zr parameters and that we predict the majority of the energy differences to come from the unique Li configurations we believed that excluding non-Li elements may still be sufficient to energetically order our structures. The only appropriate method we found was the COMPASSIII forcefield when applied to only the Li-sublattice (c.f. figure S2h). It was able to order the 13:43 with a correlation coefficient of 0.991. Given the success of COMPASSIII we sought to use it on a wider range of structures (c.f. figure S3).

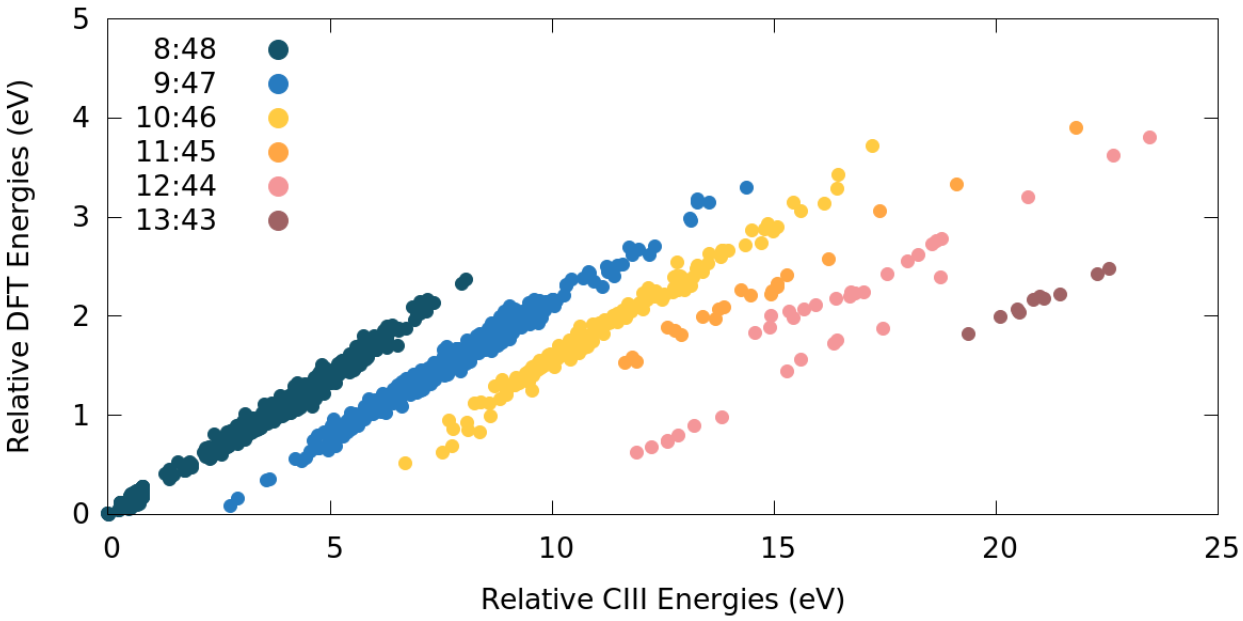

Figure S3: A comparison of 1235 relative DFT energies (found with settings described in SI section) to that of COMPASSIII

Figure S3 shows that COMPASSIII predicts a more pronounced separation of energies depending on the $24d$:$96h$ ratio than is predicted by ONETEP, while good intra-ratio ordering is retained. This issue was considered too large to surmount in this paper and we developed the multiple linear regression model presented in the main text instead.

ONETEP details

The following settings were used for our ONETEP calculations:

- Functional: PBE
- Kinetic Energy Cut-off: 830 eV
- Pseudopotentials: CASTEP on-the-fly generated pseudopotentials[58]
- NGWF Radii:
  - Li: 9.0 bohr
  - La: 10.0 bohr
  - Zr: 10.0 bohr
  - O: 9.0 bohr
- NGWF number:
  - Li: 5
  - La: 17
  - Zr: 10
  - O: 5

Dimer in Vacuum

To find the optimal inter atomic distance of a Li-dimer we performed 30 single-point calculations in a large unit cell to prevent self-interaction. We use the same, relevant, settings as used in SI section

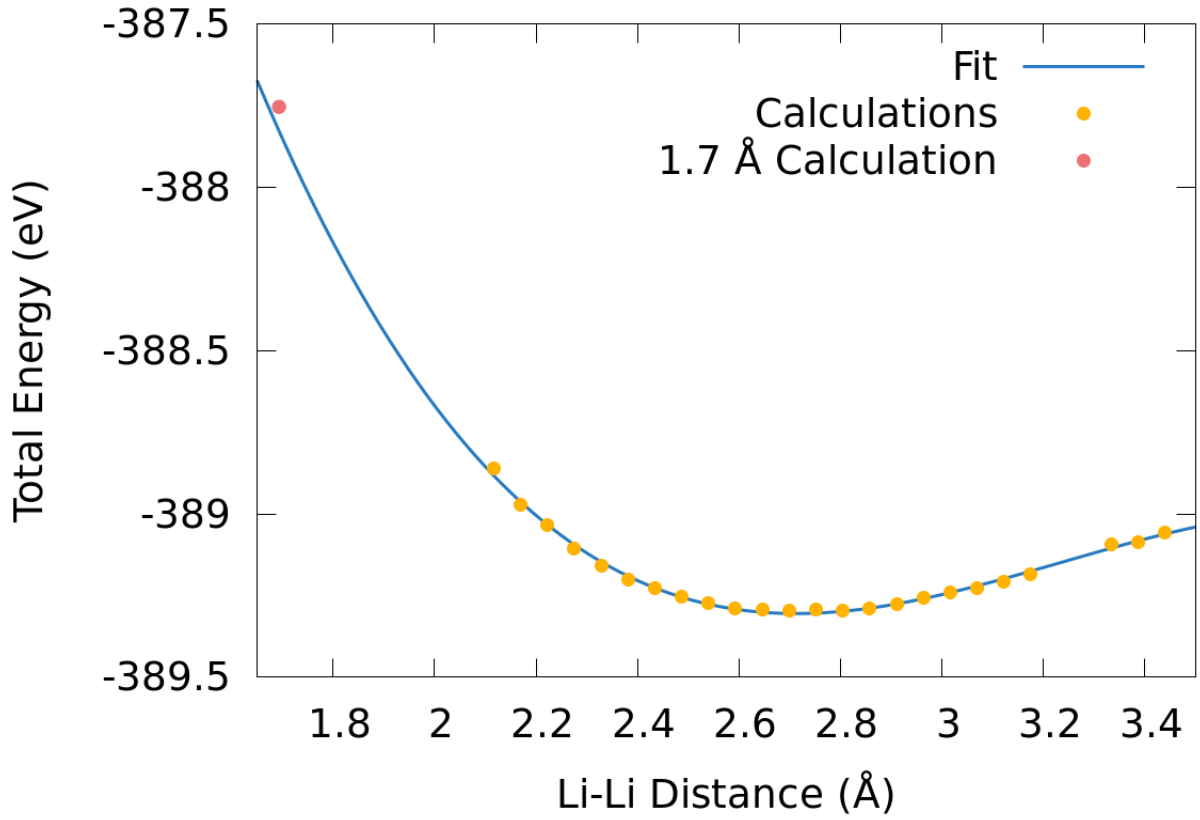

Figure S4: The energy of a Li Dimer with changing inter-atomic distance, the fit being a 3rd order polynomial of the calculations close to the optimal distance (yellow). the 1.7 Å calclulation (red) is displayed for comparison.

Using the fit in figure S4 we find the minimum energy likely to occur at approximately 2.7 Å. We also observe the large energy penalty for Li atoms approaching 1.7 Å of eachother.

Symmetry

Symmetry Checking

To validate our symmetry checking methodology we compare our results against that of more rigorous methods.[48] We use the atomic simulation environment (ASE) python package's symmetry equivalence check on the two smallest $24d$:$96h$ ratios (c.f. table 1): 12:44 and 13:43.

In both cases the same number of structures were produced using either method. Both scripts are provided with our database in SI section .

Symmetry Against Energy

Each generated c-LLZO structure will have a symmetry that is a reduced version of the *Ia3d* space group of the general crystal. We have assigned the new space groups for all 2×10^6 symmetry unique structures, knowing the group we can plot the order of the group against the predicted multiple linear regression (MLR) energy

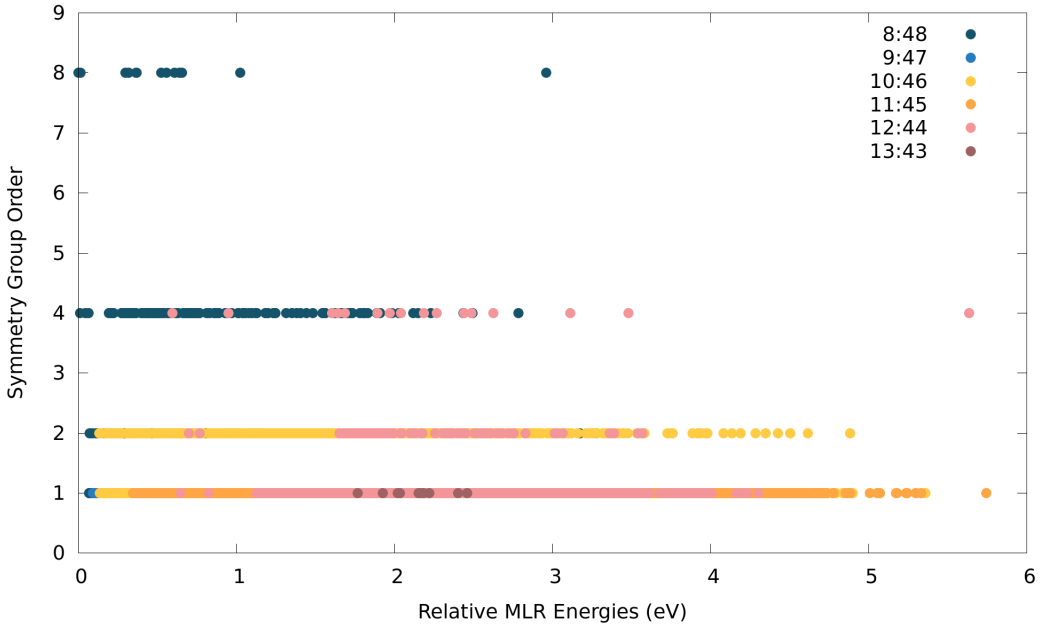

Figure S5: MLR energies compared to the order of the individual structure space group, for each $24d$:$96h$

The most symmetric ratio appears to be 8:48 followed by 12:44 and finally 10:46 with very few odd numbered $24d$ occupancies having more symmetry operations higher than 1 (the identity). there does appear to be a slight correlation between lower energy and higher symmetry.

We tested including the symmetry of the structure in our MLR model but found it made a negligible difference to overall results.

Geometry Optimisations

To assess what effect the geometry relaxed structures have on the overall ordering and also to compare our low energy structures to that of a random selection we perform 20 geometry optimisation calculations. We use the settings outlined in SI section as well as the following geometry optimisation settings for the Broyder-Fletcher-Goldfarb-Shanno (BFGS)[65] optimisation algorithm

- Energy tolerance: 1.0E-6 hartree
- Force tolerance: 0.002 ha/bohr
- Displacement tolerance: 0.005 bohr

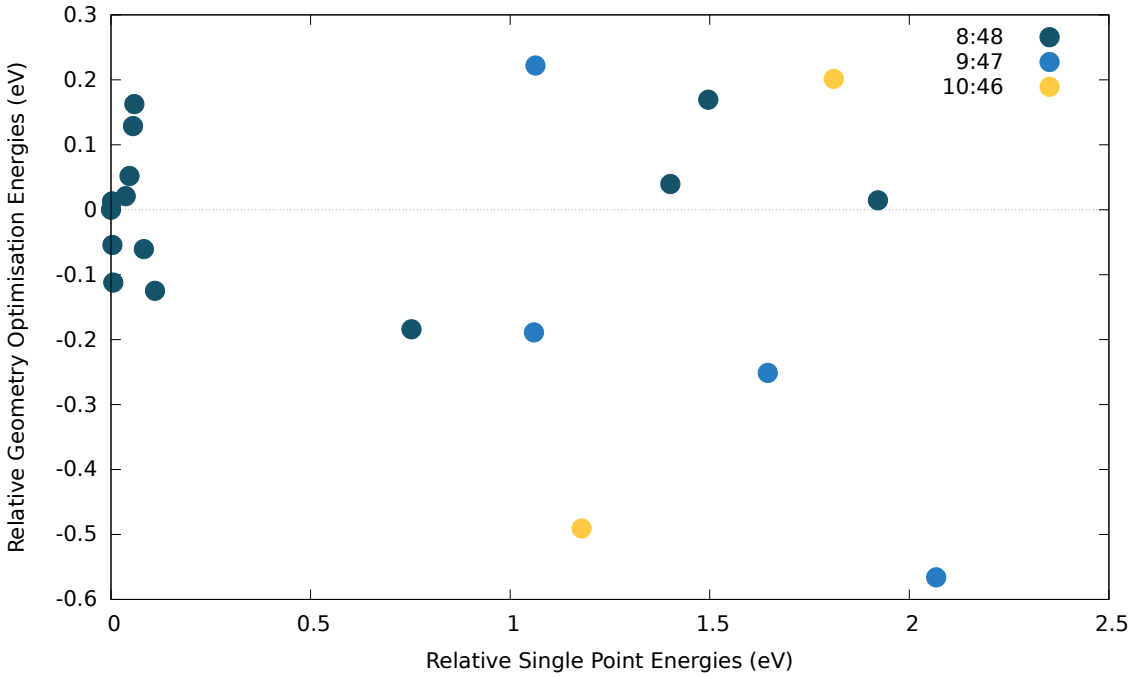

Figure S6: A comparison of the energetic ordering of 10 lowest structures according to MLR and 10 random structures for single point (SP) and geometry optimisation (GO) calculations. All energies are relative to the 355474 result for each calculation type

Figure S6 demonstrates no correlation between the single point structures and their geometry optimised counterparts. We observe three types of site change upon relaxation.

96h to 96h, 96h to 48g and 96h to 24d listed in order of frequency occurred. None of these site changes correlated significantly with the geometry optimised energy. The 96h to 24d transition was only recorded once and yielded our lowest overall energy structure (structure label 1095859): 0.58 eV lower in energy than the geometry optimised lowest energy single point structure. The 96h to 24d transition meant that the ratio of the structure changed from 9:47 to 10:46, the only time we have observed such a feature.

In figure S7a there is a negative correlation between the mean distance moved of all Li atoms in the c-LLZO structure and increasing energy of the final optimised c-LLZO structure. This indicates that the more the Li atoms move from their original crystallographic site the lower in energy the structure. Figure S7b shows a weaker negative correlation between distance to a crystallographic site and energy. These results indicate that from the structures assessed movement from original sites is preferable to attain lower energies and movement to another site is not necessary in order to attain a lower energy structure.

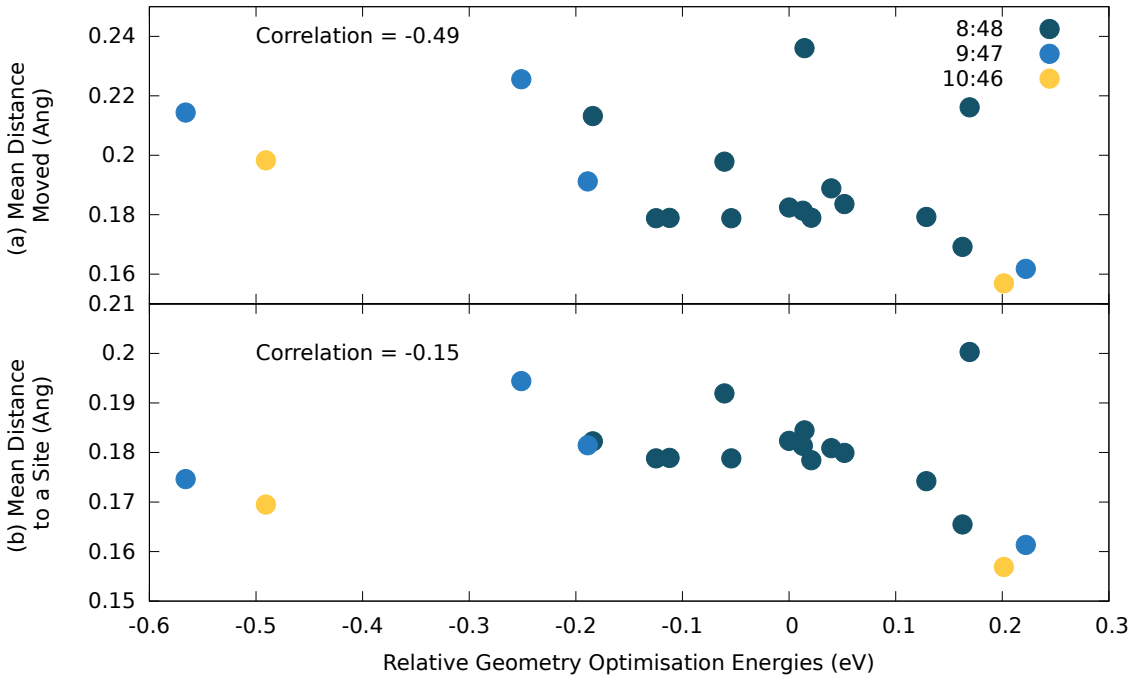

Figure S7: The relationships of the energy of 20 geometry optimised c-LLZO structures with (a) the mean distance moved by the individual Li atoms from their original crystallographically predicted site and (b) the mean distance of all Li atoms from a crystallographically identified Li site. Colours identify the 24d:96h ratio of the starting structure.

References

(1) Bates, J. B.; Dudney, N. J.; Neudecker, B.; Ueda, A.; Evans, C. D. *Thin-film lithium and lithium-ion batteries*; 2000; Vol. 135; pp 33–45.

(2) Morgan, L. M.; Mercer, M. P.; Bhandari, A.; Peng, C.; Islam, M. M.; Yang, H.; Holland, J.; Coles, S. W.; Sharpe, R.; Walsh, A. et al. Pushing the boundaries of lithium battery research with atomistic modelling on different scales. *Progress in Energy* **2022**, *4*, 012002.

(3) Dirican, M.; Yan, C.; Zhu, P.; Zhang, X. Composite solid electrolytes for all-solid-state lithium batteries. *Materials Science and Engineering: R: Reports* **2019**, *136*, 27–46.

(4) Fu, C.; Venturi, V.; Kim, J.; Ahmad, Z.; Ells, A. W.; Viswanathan, V.; Helms, B. A. Universal chemomechanical design rules for solid-ion conductors to prevent dendrite formation in lithium metal batteries. *Nature Materials* **2020**, *19*, 758–766.

(5) Sudo, R.; Nakata, Y.; Ishiguro, K.; Matsui, M.; Hirano, A.; Takeda, Y.; Yamamoto, O.; Imanishi, N. Interface behavior between garnet-type lithium-conducting solid electrolyte and lithium metal. *Solid State Ionics* **2014**, *262*, 151–154.

(6) Canepa, P.; Dawson, J. A.; Sai Gautam, G.; Statham, J. M.; Parker, S. C.; Islam, M. S. Particle Morphology and Lithium Segregation to Surfaces of the Li7La3Zr2O12 Solid Electrolyte. *Chemistry of Materials* **2018**, *30*, 3019–3027.

(7) Barai, P.; Ngo, A. T.; Narayanan, B.; Higa, K.; Curtiss, L. A.; Srinivasan, V. The Role of Local Inhomogeneities on Dendrite Growth in LLZO-Based Solid Electrolytes. *Journal of The Electrochemical Society* **2020**, *167*, 100537.

(8) Gao, Y.; Nolan, A. M.; Du, P.; Wu, Y.; Yang, C.; Chen, Q.; Mo, Y.; Bo, S. H. Classical and Emerging Characterization Techniques for Investigation of Ion Transport Mechanisms in Crystalline Fast Ionic Conductors. *Chemical Reviews* **2020**, *120*, 5954–6008.

(9) Tian, H.-K.; Xu, B.; Qi, Y. Computational study of lithium nucleation tendency in Li7La3Zr2O12 (LLZO) and rational design of interlayer materials to prevent lithium dendrites. *Journal of Power Sources* **2018**, *392*, 79–86.

(10) Zhu, Y.; He, X.; Mo, Y. Origin of Outstanding Stability in the Lithium Solid Electrolyte Materials: Insights from Thermodynamic Analyses Based on First-Principles Calculations. *ACS Applied Materials & Interfaces* **2015**, *7*, 23685–23693.

(11) Awaka, J.; Kijima, N.; Hayakawa, H.; Akimoto, J. Synthesis and structure analysis of tetragonal Li7La3Zr2O12 with the garnet-related type structure. *Journal of Solid State Chemistry* **2009**, *182*, 2046–2052.

(12) Awaka, J.; Takashima, A.; Kataoka, K.; Kijima, N.; Idemoto, Y.; Akimoto, J. Crystal Structure of Fast Lithium-ion-conducting Cubic Li ¡sub¿7¡/sub¿ La ¡sub¿3¡/sub¿ Zr ¡sub¿2¡/sub¿ O ¡sub¿12¡/sub¿. *Chemistry Letters* **2011**, *40*, 60–62.

(13) Geiger, C. A.; Alekseev, E.; Lazic, B.; Fisch, M.; Armbruster, T.; Langner, R.; Fechtelkord, M.; Kim, N.; Pettke, T.; Weppner, W. Crystal chemistry and stability of "Li7La 3Zr2O12" garnet: A fast lithium-ion conductor. *Inorganic Chemistry* **2011**, *50*, 1089–1097.

(14) Kumazaki, S.; Iriyama, Y.; Kim, K. H.; Murugan, R.; Tanabe, K.; Yamamoto, K.; Hirayama, T.; Ogumi, Z. High lithium ion conductive Li7La3Zr 2O12 by inclusion of both Al and Si. *Electrochemistry Communications* **2011**, *13*, 509–512.

(15) Shimonishi, Y.; Toda, A.; Zhang, T.; Hirano, A.; Imanishi, N.; Yamamoto, O.; Takeda, Y. Synthesis of garnet-type Li7 - XLa3Zr 2O12 - 1/2x and its stability in aqueous solutions. *Solid State Ionics* **2011**, *183*, 48–53.

(16) Rangasamy, E.; Wolfenstine, J.; Sakamoto, J. The role of Al and Li concentration on the formation of cubic garnet solid electrolyte of nominal composition Li7La3Zr2O12. *Solid State Ionics* **2012**, *206*, 28–32.

(17) Xie, H.; Alonso, J. A.; Li, Y.; Fernández-Díaz, M. T.; Goodenough, J. B. Lithium Distribution in Aluminum-Free Cubic Li 7 La 3 Zr 2 O 12. *Chemistry of Materials* **2011**, *23*, 3587–3589.

(18) Brugge, R. H.; Kilner, J. A.; Aguadero, A. Germanium as a donor dopant in garnet electrolytes. *Solid State Ionics* **2019**, *337*, 154–160.

(19) Buschmann, H.; Dölle, J.; Berendts, S.; Kuhn, A.; Bottke, P.; Wilkening, M.; Heitjans, P.; Senyshyn, A.; Ehrenberg, H.; Lotnyk, A. et al. Structure and dynamics of the fast lithium ion conductor "li 7La3Zr2O12". *Physical Chemistry Chemical Physics* **2011**, *13*, 19378–19392.

(20) Hiebl, C.; Young, D.; Wagner, R.; Wilkening, H. M.; Redhammer, G. J.; Rettenwander, D. Proton Bulk Diffusion in Cubic Li 7 La 3 Zr 2 O 12 Garnets as Probed by Single X-ray Diffraction. *Journal of Physical Chemistry C* **2019**, *123*, 1094–1098.

(21) Wagner, R.; Redhammer, G. J.; Rettenwander, D.; Senyshyn, A.; Schmidt, W.; Wilkening, M.; Amthauer, G. Crystal Structure of Garnet-Related Li-Ion Conductor Li7-3xGaxLa3Zr2O12: Fast Li-Ion Conduction Caused by a Different Cubic Modification? *Chemistry of Materials* **2016**, *28*, 1861–1871.

(22) Rettenwander, D.; Redhammer, G.; Preishuber-Pflügl, F.; Cheng, L.; Miara, L.; Wagner, R.; Welzl, A.; Suard, E.; Doeff, M. M.; Wilkening, M. et al. Structural and Electrochemical Consequences of Al and Ga Cosubstitution in Li7La3Zr2O12 Solid Electrolytes. *Chemistry of Materials* **2016**, *28*, 2384–2392.

(23) Robben, L.; Merzlyakova, E.; Heitjans, P.; Gesing, T. M. Symmetry reduction due to gallium substitution in the garnet Li6.43(2)Ga0.52(3)La2.67(4)Zr2O12. *Acta Crystallographica Section E: Crystallographic Communications* **2016**, *72*, 287–289.

(24) Howard, M. A.; Clemens, O.; Kendrick, E.; Knight, K. S.; Apperley, D. C.; Ander-

son, P. A.; Slater, P. R. Effect of Ga incorporation on the structure and Li ion conductivity of La3Zr2Li7O12. *Dalton Transactions* **2012**, *41*, 12048–12053.

(25) Yu, S.; Schmidt, R. D.; Garcia-Mendez, R.; Herbert, E.; Dudney, N. J.; Wolfenstine, J. B.; Sakamoto, J.; Siegel, D. J. Elastic Properties of the Solid Electrolyte Li7La3Zr2O12 (LLZO). *Chemistry of Materials* **2016**, *28*, 197–206.

(26) Thompson, T.; Yu, S.; Williams, L.; Schmidt, R. D.; Garcia-Mendez, R.; Wolfenstine, J.; Allen, J. L.; Kioupakis, E.; Siegel, D. J.; Sakamoto, J. Electrochemical Window of the Li-Ion Solid Electrolyte Li 7 La 3 Zr 2 O 12. *ACS Energy Letters* **2017**, *2*, 462–468.

(27) Sharafi, A.; Kazyak, E.; Davis, A. L.; Yu, S.; Thompson, T.; Siegel, D. J.; Dasgupta, N. P.; Sakamoto, J. Surface Chemistry Mechanism of Ultra-Low Interfacial Resistance in the Solid-State Electrolyte Li7La3Zr2O12. *Chemistry of Materials* **2017**, *29*, 7961–7968.

(28) Yu, S.; Siegel, D. J. Grain Boundary Contributions to Li-Ion Transport in the Solid Electrolyte Li7La3Zr2O12 (LLZO). *Chemistry of Materials* **2017**, *29*, 9639–9647.

(29) Rettenwander, D.; Blaha, P.; Laskowski, R.; Schwarz, K.; Bottke, P.; Wilkening, M.; Geiger, C. A.; Amthauer, G. DFT study of the role of Al3+ in the fast ion-conductor Li 7-3xAl3+xLa3Zr2O 12 garnet. *Chemistry of Materials* **2014**, *26*, 2617–2623.

(30) Xu, M.; Park, M. S.; Lee, J. M.; Kim, T. Y.; Park, Y. S.; Ma, E. Mechanisms of Li ¡math display="inline"¿ ¡msup¿ ¡mrow/¿ ¡mo¿+¡/mo¿ ¡/msup¿ ¡/math¿ transport in garnet-type cubic Li ¡math display="inline"¿ ¡msub¿ ¡mrow/¿ ¡mrow¿ ¡mn¿3¡/mn¿ ¡mo¿+¡/mo¿ ¡mi¿x¡/mi¿ ¡/mrow¿ ¡/msub¿ ¡/math¿ La ¡math display="inline"¿ ¡mrow¿ ¡msub¿ ¡mrow/¿ ¡mn¿3¡/mn¿ ¡/msub¿ ¡msub¿ ¡mi¿M¡/mi¿ ¡mn¿2¡/mn¿ ¡/msub¿ ¡/mrow¿ ¡/math¿ O ¡math display="inline"¿ ¡msub¿ ¡mrow/¿ ¡mn¿12¡/mn¿ ¡/msub¿

¡/math¿ (¡math display=”inline”¿ ¡mi¿M¡/mi¿ ¡/math¿ = Te, Nb, Zr). *Physical Review B* **2012**, *85*, 052301.

(31) Jalem, R.; Yamamoto, Y.; Shiiba, H.; Nakayama, M.; Munakata, H.; Kasuga, T.; Kanamura, K. Concerted migration mechanism in the Li ion dynamics of garnet-type Li 7La3Zr2O12. *Chemistry of Materials* **2013**, *25*, 425–430.

(32) Meier, K.; Laino, T.; Curioni, A. Solid-state electrolytes: Revealing the mechanisms of Li-Ion conduction in tetragonal and cubic LLZO by first-principles calculations. *Journal of Physical Chemistry C* **2014**, *118*, 6668–6679.

(33) Santosh, K. C.; Longo, R. C.; Xiong, K.; Cho, K. Point defects in garnet-type solid electrolyte (c-Li7La 3Zr2O12) for Li-ion batteries. *Solid State Ionics* **2014**, *261*, 100–105.

(34) Verduzco, J. C.; Marinero, E. E.; Strachan, A. Atomistic Mechanisms Underlying the Maximum in Diffusivity in Doped Li ¡sub¿7¡/sub¿ La ¡sub¿3¡/sub¿ Zr ¡sub¿2¡/sub¿ O ¡sub¿12¡/sub¿. *The Journal of Physical Chemistry C* **2023**, *127*, 10806–10812.

(35) Haarmann, L.; Rohrer, J.; Albe, K. On the Origin of Zero Interface Resistance in the Li6.25Al0.25La3Zr2O12—Li0System: An Atomistic Investigation. *ACS Applied Materials and Interfaces* **2021**, *13*, 52629–52635.

(36) Shannon, R. D. *Revised Effective Ionic Radii and Systematic Studies of Interatomie Distances in Halides and Chaleogenides*; 1976; Vol. 32; p 751.

(37) Bijvoet, J. M. A.; Keesom, W. H. The scattering power of lithium and oxygen, determined from the diffraction-intensities of powdered lithiumoxide. *Proceedings of the Koninklijke Nederlandse Academie van Wetenschappen* **1926**, *29*, 1286– 1292.

(38) Barrett, C. S. A Low Temperature Transformation in Lithium. *Physical Review* **1947**, *72*, 245–245.

(39) Kumar, N.; Seminario, J. M. Lithium-ion model behavior in an ethylene carbonate electrolyte using molecular dynamics. *Journal of Physical Chemistry C* **2016**, *120*, 16322–16332.

(40) Zhang, X.; Liu, W.; Yu, Y. The effects of local strain on the cubic Li7La3Zr2O12(001)/Li(001) interface: A first-principles study. *Solid State Ionics* **2021**, *360*.

(41) Ajith, K.; Christopher Selvin, P.; Abhilash, K.; Sivaraj, P.; Nalini, B.; Soundarya, G. A correlative study on electrochemical and optical properties of LLZO (Li7La3Zr2O12) garnet electrolyte. *Materials Today: Proceedings* **2022**, *50*, 2836–2839.

(42) Sazvar, A.; Sarpoolaky, H.; Golmohammad, M. The effects of electric field on physical properties of LLZO made by flash sintering method. *Solid State Ionics* **2022**, *386*.

(43) Lee, K.; Kazyak, E.; Wang, M. J.; Dasgupta, N. P.; Sakamoto, J. Analyzing void formation and rewetting of thin in situ-formed Li anodes on LLZO. *Joule* **2022**, *6*, 2547–2565.

(44) Fuchs, T.; Becker, J.; Haslam, C. G.; Lerch, C.; Sakamoto, J.; Richter, F. H.; Janek, J. Current-Dependent Lithium Metal Growth Modes in "Anode-Free" Solid-State Batteries at the Cu—LLZO Interface. *Advanced Energy Materials* **2023**, *13*.

(45) Cussen, E. J. The structure of lithium garnets: cation disorder and clustering in a new family of fast Li ¡sup¿+¡/sup¿ conductors. *Chem. Commun.* **2006**, 412–413.

(46) Ricci, F.; Chen, W.; Aydemir, U.; Snyder, G. J.; Rignanese, G.-M.; Jain, A.; Hautier, G. An ab initio electronic transport database for inorganic materials. *Scientific Data* **2017**, *4*, 170085.

(47) Leskovec, J.; Rajaraman, A.; Ullman, J. D. *Mining of massive datasets*, 2nd ed.; Cambridge University Press: Cambridge, 2014.

(48) Togo, A.; Oba, F.; Tanaka, I. First-principles calculations of the ferroelastic transition between rutile-type and CaCl2-type SiO2 at high pressures. *Physical Review B - Condensed Matter and Materials Physics* **2008**, *78*, 1–9.

(49) Bhandari, A.; Jindal, P.; Bhattacharya, J. Discovery of new ground state structures for Li4Mn2O5 and V2O5 from first principles. *Computational Materials Science* **2019**, *159*, 454–459.

(50) Van der Ven, A.; Thomas, J.; Puchala, B.; Natarajan, A. First-Principles Statistical Mechanics of Multicomponent Crystals. *Annual Review of Materials Research* **2018**, *48*, 27–55.

(51) Akkermans, R. L. C.; Spenley, N. A.; Robertson, S. H. COMPASS III: automated fitting workflows and extension to ionic liquids. *Molecular Simulation* **2021**, *47*, 540–551.

(52) Prentice, J. C. A.; Aarons, J.; Womack, J. C.; Allen, A. E. A.; Andrinopoulos, L.; Anton, L.; Bell, R. A.; Bhandari, A.; Bramley, G. A.; Charlton, R. J. et al. The ONETEP linear-scaling density functional theory program. *The Journal of Chemical Physics* **2020**, *152*, 174111.

(53) Skylaris, C.-K.; Haynes, P. D.; Mostofi, A. A.; Payne, M. C. Introducing ¡scp¿ONETEP¡/scp¿ : Linear-scaling density functional simulations on parallel computers. *The Journal of Chemical Physics* **2005**, *122*, 084119.

(54) Perdew, J. P.; Burke, K.; Wang, Y. Generalized gradient approximation for the exchange-correlation hole of a many-electron system. *Physical Review B* **1996**, *54*, 16533–16539.

(55) Sharafi, A.; Yu, S.; Naguib, M.; Lee, M.; Ma, C.; Meyer, H. M.; Nanda, J.; Chi, M.; Siegel, D. J.; Sakamoto, J. Impact of air exposure and surface chemistry on Li-Li7La3Zr2O12 interfacial resistance. *Journal of Materials Chemistry A* **2017**, *5*, 13475–13487.

(56) Okhotnikov, K.; Charpentier, T.; Cadars, S. Supercell program: A combinatorial structure-generation approach for the local-level modeling of atomic substitutions and partial occupancies in crystals. *Journal of Cheminformatics* **2016**, *8*.

(57) Elstner, M.; Porezag, D.; Jungnickel, G.; Elsner, J.; Haugk, M.; Frauenheim, T. Self-consistent-charge density-functional tight-binding method for simulations of complex materials properties. *Physical Review B - Condensed Matter and Materials Physics* **1998**, *58*, 7260–7268.

(58) Clark, S. J.; Segall, M. D.; Pickard, C. J.; Hasnip, P. J.; Probert, M. I.; Refson, K.; Payne, M. C. First principles methods using CASTEP. *Zeitschrift fur Kristallographie* **2005**, *220*, 567–570.

(59) BIOVIA, Dassault Systemes, Materials Studio, 23.1.0.3829, San Diego: Dassault Systemes. 2023.

(60) Rappe, A. K.; Casewit, C. J.; Colwell, K. S.; Goddard, W. A.; Skiff, W. M. UFF, a full periodic table force field for molecular mechanics and molecular dynamics simulations. *Journal of the American Chemical Society* **1992**, *114*, 10024–10035.

(61) Hourahine, B.; Aradi, B.; Blum, V.; Bonafé, F.; Buccheri, A.; Camacho, C.; Cevallos, C.; Deshaye, M. Y.; Dumitrică, T.; Dominguez, A. et al. DFTB+, a software package for efficient approximate density functional theory based atomistic simulations. *The Journal of Chemical Physics* **2020**, *152*, 124101.

(62) Sun, H. COMPASS: An ab Initio Force-Field Optimized for Condensed-Phase ApplicationsOverview with Details on Alkane and Benzene Compounds. *The Journal of Physical Chemistry B* **1998**, *102*, 7338–7364.

(63) Hagler, A. T.; Huler, E.; Lifson, S. Energy functions for peptides and proteins. I. Derivation of a consistent force field including the hydrogen bond from amide crystals. *Journal of the American Chemical Society* **1974**, *96*, 5319–5327.

(64) Sun, H.; Mumby, S. J.; Maple, J. R.; Hagler, A. T. An ab Initio CFF93 All-Atom Force Field for Polycarbonates. *Journal of the American Chemical Society* **1994**, *116*, 2978–2987.

(65) Shanno, D. F. Conjugate Gradient Methods with Inexact Searches. *Mathematics of Operations Research* **1978**, *3*, 244–256.